Effect of Alloying on the Fermi Surface of Beryllium*

J. H. Tripp,† P. M. Everett,‡ J. M. Fiske, and W. L. Gordon
Department of Physics, Case Western Reserve University, Cleveland, Ohio 44106
(Received 30 March 1970)

The Fermi surfaces of some dilute (less than 1 at.%) alloys of beryllium with copper have been measured by the de Haas–van Alphen (dHvA) effect with an accuracy of about ½%. Some cyclotron masses have also been obtained. For comparison with experiment, the nonlocal-pseudopotential model for the Fermi surface of pure beryllium has been extended to include dilute random substitutional alloys. It is found that the changes in the Fermi surface arise principally from the shift of Fermi level and the lattice-spacing changes, while the effect of including explicitly the solute pseudopotential appears to be unimportant for these dilute alloys. The only adjustable parameter in each alloy is the Fermi level, and this is determined by fitting a single measured de Haas–van Alphen frequency. The model Fermi surface thus produced fits all the observed dHvA frequencies with an accuracy of about 1%, comparable with the accuracy of the pure-beryllium model.

I. INTRODUCTION

In a previous paper,[1] to be referred to as I, a nonlocal pseudopotential model for the Fermi surface (FS) of beryllium has been described, and it is the purpose of the present work to extend this model and to apply it to dilute alloys. The FS of beryllium is well suited to a study of changes by alloying with solutes from adjacent columns of the Periodic Table because the electron and hole volumes are initially small (0.016 states/atom). Thus, it is quite sensitive to change in electron concentration. Figure 1, taken from I, shows the FS which is consistent with the model and data presented there. de Haas–van Alphen (dHvA) measurements have been made on some copper alloys and observed and calculated frequencies are found to agree within 1% in most cases. This indicates that, at least for dilute alloys, the model contains all the more important features of alloying. For higher concentrations, there are clearly additional effects to be considered but, at these concentrations, the dHvA signals grow very weak because of impurity scattering of the conduction electrons. For those reasons, the present model provides a description of dilute alloys only.

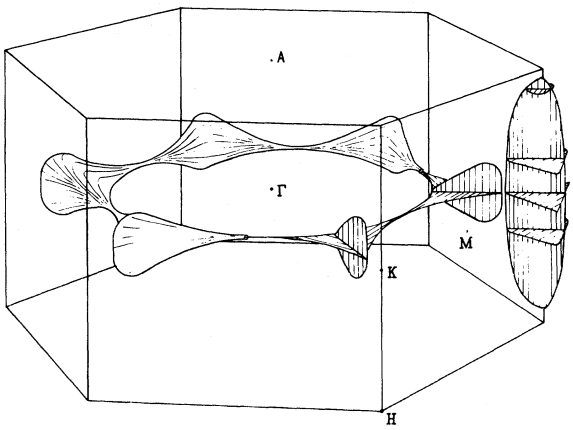

FIG. 1. Second-band hole surface (coronet) and one-half of the third-band electron surface (cigar) of beryllium. The volumes of electrons and holes are equal, about 0.8% of the volume of the first Brillouin zone or 0.016 states/atom.

The pseudopotential formulation used in I for the pure metal was semiempirical in the sense that certain parameters were adjusted by fitting to experimental dHvA data. For alloys, the parameters are derived from their pure metal values in a well-defined manner, but since the volume of the FS changes with composition, it is necessary to find the Fermi level by fitting a single frequency to its observed value. This suffices to provide the complete FS. The properties of the individual solute atoms enter the model in two ways: through their influence on the lattice spacings and through the change in electron concentration. Their effect on the lattice potential is not otherwise taken into account in this model.

The experimental work is presented in Sec. II, while Sec. III introduces the theoretical model together with a simple expression for rapidly estimating the effects of alloying. The results are given and discussed in Sec. IV.

II. EXPERIMENTAL RESULTS

The alloy samples were purchased from the Franklin Institute in the form of a single-crystal rod with several different copper concentrations zone levelled at separate locations along the rod.

Experimental samples having the necessary orientations were cut from the rod by spark erosion and the concentration obtained by chemical analysis of cutting scraps. The uncertainty in concentration is approximately ±10% of the nominal value quoted. Uniformity of composition was tested in several of these scraps at the electron microprobe facility at the CWRU Materials Center and was found to be satisfactory down to a scale of approximately 20 μ. Typically, the samples were cubes, ~2.5 mm on a side, but in some cases cut to a larger size. There was surprisingly little lineage compared to the usual pure beryllium with $<\frac{1}{2}^\circ$ spread as estimated from back-reflection Laue patterns. The lattice parameters for each alloy were obtained, on the assumption of a linear variation with concentration, from the room-temperature data for pure beryllium and for a 0.64 at.% copper alloy. These values are listed in Table I.

The dHvA frequencies reported here were obtained by techniques identical to those reported in I: field modulation in fields up to 60 kG and a torque magnetometer at lower fields. These techniques are described in more detail in Ref. 2. Oscillation amplitudes were low compared to pure beryllium since they should depend on concentration as $e^{-C\eta/H}$, where C is a constant, η the concentration of copper, and H the applied field. Thus, high magnetic fields were required so that most of the data were taken in the 60-kG solenoid using a modulation method. Representative cyclotron masses for several portions of the FS were obtainable in only the lowest alloy concentration. Where more than one dHvA frequency was observable, the precautions of Ref. 2 were followed in extracting masses. It was possible to extend these measurements to higher concentrations only for the family of lowest dHvA frequencies.

TABLE I. Lattice constants.

	c(Å)	a(Å)
Pure Be (300 °K)[a]	3.5844	2.2855
(0 °K)[b]	3.5814	2.2828
Be+0.64 at.% Cu (300 °K)[a]	3.5911	2.2836
Be+0.08 at. % Cu (0 °K)[c]	3.5822	2.2826
Be+0.4 at.% Cu (0 °K)[c]	3.5856	2.2816
Be+0.78 at.% Cu (0 °K)[c]	3.5895	2.2805

[a]G. London (private communication).

[b]Thermal expansion data of R. W. Meyerhoff and J. P. Smith [J. Appl. Phys. 33, 219 (1962)] were used in an extrapolation to 0 °K.

[c]In calculating these values, it was assumed that over this concentration range the room-temperature lattice constants vary linearly with copper concentration and that the thermal contraction to 0 °K would be identical with pure beryllium.

Results for frequency branches originating from three portions of the FS are shown in Figs. 2 and 3 for the 0.08 at.% Cu alloy where they are compared with the angular dependence for pure beryllium. The notation is the same as that employed in I: Greek letters denote frequency branches arising from electron orbits on common portions of the FS with a subscript specifying the crystalline plane in which the magnetic field lies [1 for $(10\bar{1}0)$, 2 for $(11\bar{2}0)$, and 3 for (0001)] and a superscript denoting the individual branch. Orbits on the cigar are designated α, while β and γ refer, respectively, to orbits on the belly and neck of the coronet.

At higher alloy concentrations, the amplitude of the α oscillations was below the noise level of the apparatus. The α oscillations were unobservable in the 0.78 at.% alloy and very weak in the 0.41 at.% Cu alloy. Here, their angular dependence was similar to that of pure Be and to the 0.08 at.% Cu alloy in the range $0<\theta<30^\circ$ over which they were above noise level, but there was no observable beat pattern. Thus, in sweeping the field down from 60 kG through 60 oscillations to a point where the signal was virtually lost in the noise, no evidence of a beat waist was seen. This places an estimated upper limit on the amplitude of the second component as approximately $\frac{1}{10}$ of the dominant component or on the frequency difference between the two components as about 1 part in 100. A possible explanation for the absence of the beat will be discussed later.

The γ oscillations were observed by the torque method in alloys as concentrated as 0.78 at.% Cu, but showed no unusual angular dependence. Therefore, the results for concentrations greater than 0.08 at.% Cu are tabulated for symmetry directions only and presented later with the corresponding computed values.

III. ALLOY MODELS

Following the method described in I, a nonlocal pseudopotential for calculating the energy levels of a pure metal may be derived from the orthogonalized-plane-wave (OPW) formulation by combining the orthogonalizing terms in the Schrödinger equation with the usual Hamiltonian H. This approach has been described by Harrison[3] and leads to the pseudo-Hamiltonian

$$\vec{H} = H + \sum_\alpha (E - E_\alpha)(|\alpha\rangle\langle\alpha|/\langle\alpha|\alpha\rangle) , \qquad (1)$$

where the atomic core states $|\alpha\rangle$ satisfy

$$H|\alpha\rangle = E_\alpha|\alpha\rangle . \qquad (2)$$

In the pure crystal, the core states $|\alpha\rangle$ to which the conduction states are orthogonalized may be

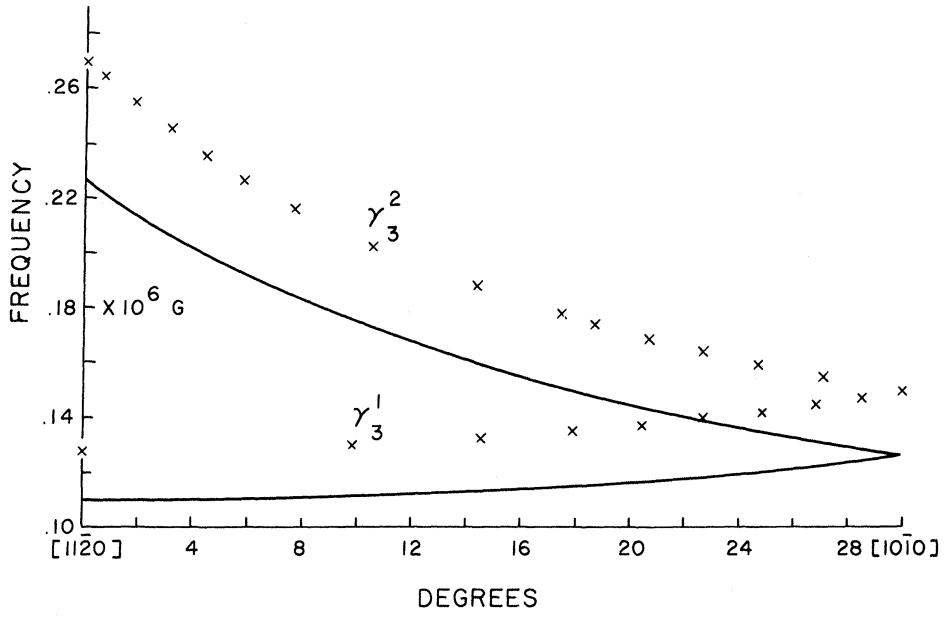

FIG. 2. Comparison of dHvA frequencies arising from extremal orbits on the "neck" of the coronet in pure Be (solid line) and in the 0.08 at. % Cu alloy (x points) for H in the (0001) plane.

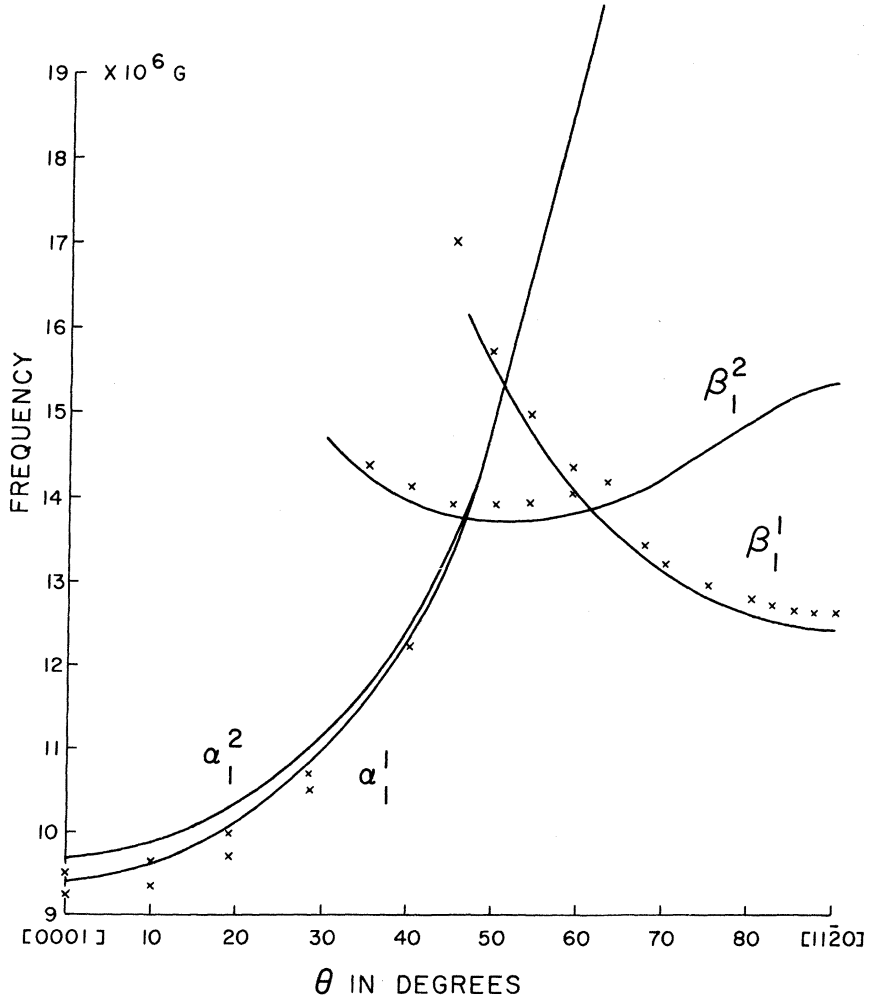

FIG. 3. Comparison of results for pure Be (solid line) and for the 0.08 at. % Cu (x points) for extremal orbits on the "cigar" and on the "belly" of the coronet.

regarded either as extended Bloch states such as the linear combinations of atomic orbitals (LCAO's) constructed from the atomic functions at each site or as the individual localized atomic core states themselves. In the first representation, the suffix α runs only over the various occupied levels of a single atom, while in the second, α designates also the position $\vec{R}_n$ of the atom. Both representations yield the same form for the matrix elements of $\tilde{H}$ in the small-core approximation.

In a random substitutional alloy, however, the core functions have an explicit dependence on $\vec{R}_n$ and the construction of Bloch functions is no longer possible because translational symmetry is destroyed. It becomes necessary to adopt the second approach and to orthogonalize to the individual atomic cores.

Let us define

$$w_n(\vec{k}_{ij}) = v_n(\vec{k}_{ij}) + \sum_{\alpha_n} [E(\vec{k}) - E_\alpha^n] \frac{\langle \vec{k}_i | \alpha_n \rangle \langle \alpha_n | \vec{k}_j \rangle}{\langle \alpha_n | \alpha_n \rangle} , \quad (3)$$

where $\vec{k}_{ij} = \vec{k}_i - \vec{k}_j$ is the difference between two $\vec{k}$ vectors defining plane-wave conduction states $|\vec{k}\rangle$. The Fourier transforms of the atomiclike potential and atomic core state $|\alpha_n\rangle$ at site n are denoted, respectively, by $v_n(\vec{k}_{ij})$ and $\langle \vec{k}_i | \alpha_n \rangle$ while E_α^n is the corresponding core energy level. $E(\vec{k})$ is the conduction level we seek. Thus, $w_n(\vec{k})$ is an atomiclike pseudopotential form factor in terms of which the plane-wave matrix elements of $\tilde{H}$ may be written

$$\tilde{H}_{ij} = k_j^2 \delta_{ij} + \frac{1}{N\Omega_0} \sum_n e^{i\vec{k}_{ij} \cdot \vec{R}_n} w_n(\vec{k}_{ij}) . \quad (4)$$

N is the total number of atomic positions in the crystal, unit cell volume Ω_0, and the sum runs over all sites.

In the pure metal, $\tilde{H}_{ij}$ vanishes unless $\vec{k}_{ij}$ is a reciprocal-lattice vector $\vec{G}_{ij}$, because w_n is independent of n and the summation then produces the usual structure factor $S(\vec{G}_{ij})$. For beryllium, Eq. (4) then reduces to Eq. (2) of I, in which the $v(\vec{G}_{ij})$ were treated as disposable parameters. A highly accurate fit to the pure Be FS was obtained using only 12 plane waves in the expansion of the pseudo-wave-function.

In dilute alloys, on the other hand, the w_n are of course determined by the atom type at $\vec{R}_n$. Moreover, if v_n contains conduction electron screening only to first order, then w_n depends solely on the atom at $\vec{R}_n$ and also on the neighborhood[4] of $\vec{R}_n$. Each atom may thus be regarded as carrying its own pseudopotential with it in the alloy, even though this is in general different from the pseudopotential in the respective pure metal. Under these conditions, it is possible to separate the total pseudopotential into periodic and nonperiodic parts. The periodic part may be written as the sum over all sites of an atomiclike potential $w_p \equiv \sum_i \gamma_i w_i$ where summation extends over all alloy components i. The nonperiodic part will describe the electron scattering, while the periodic potential yields a band structure,[3] according to the eigenvalues of the modified pseudo-Hamiltonian matrix:

$$(\tilde{H}_p)_{ij} = k_j^2 \delta_{ij} + (1/\Omega_0)\, S(\vec{G}_{ij})\, w_p(\vec{k}_{ij}) . \quad (5)$$

The virtual-crystal model of Nordheim[5] corresponds to taking γ_i equal to the concentration of component i. In our case, where the form factor $w(\vec{k})$ for copper is not known, largely because of the intermediate nature of the d levels, it seems appropriate to take γ_{Be} as unity and γ_{Cu} as zero. For concentrations below 1 at.% Cu, this probably introduces negligible error in the band structure although the effect on the scattering part of the potential would be large.

The matrix element defined by Eqs. (3) and (5) differs in this approximation from the pure metal in several ways. The change in c and a spacing produced by alloying alters both Ω_0 and the lengths G_{ij} of the reciprocal-lattice vectors. The coefficients $v(G_{ij})$ were determined by fitting a smooth function through the pure-metal points and interpolating; the same method was used in I for calculating strain and pressure derivatives. In addition, the nonlocal part of the matrix element is altered, if we consider points on the FS, by the change in Fermi level E_F, itself due to the different number of conduction electrons present.

In the pure metal, we determine the FS by compensating the volumes of hole and electron states in the Brillouin zone. Similarly here, we could find the Fermi level by assuming an effective valency for each atom in the alloy. In I, the required accuracy in locating the Fermi level was estimated to be about 20 μRy, which means that the electron concentration must be known to about 0.002%. This, in turn, depends on screening effects as well as on the atomic concentration. It thus seemed better to find E_F by fitting one of the observed dHvA frequencies. The frequency providing the most sensitive test, and the one most readily measured, is the γ_1^1 frequency associated with the thin connecting necks of the coronet. Being the lowest frequency, it suffers least from the reduction in amplitude caused by impurity scattering.

To summarize, the calculation of the FS described here is completely specified by the lattice spacings of the alloy and a single dHvA frequency.

The required pseudopotential parameters are derived from their values in pure Be. Thus, the specific nature of the solute atoms is not directly included in the crystal potential but is felt through their valency and influence on lattice spacings. The numerical methods for computing frequencies, cyclotron masses, etc., are then the same as in I.

There is a simple expression giving an approximation for the effect of alloying on dHvA frequencies which makes use of quantities available from the pure-metal calculations alone. This has the advantage of providing a quick estimate of the changes expected for a given concentration and solute without resorting to the full computation. It also gives some physical insight into the changes of the FS. As we have seen above, our model FS depends upon the lattice spacings and the Fermi level, so that we may develop any frequency f in Taylor series in the variables c, a, and E:

$$\Delta f = \frac{\partial f}{\partial E}\Delta E + \frac{1}{2}\frac{\partial^2 f}{\partial E^2}(\Delta E)^2 + \frac{\partial f}{\partial c}\Delta c + \frac{\partial f}{\partial a}\Delta a, \quad (6)$$

where only the more significant terms are retained. The first two terms give the change due to the shift in Fermi level, ΔE. They are sometimes referred to as "fixed-band" terms since they take no account of changes in shape of the energy surfaces arising through changes in potential or cell volume. We evaluate the first term by noting that the calculated cyclotron mass gives us $\partial f/\partial E$ while ΔE is given by the change in electron concentration divided by the calculated density of states $n(E_F)$. Similarly, the second term may be obtained by calculating the variation with effective Fermi level of the pure-metal cyclotron mass. Except for frequencies arising from a nearly vanishing piece of FS such as the neck, this term can usually be ignored. Finally, the last two terms may be found from the strain and pressure derivatives given in I.

IV. RESULTS AND DISCUSSION

Three *Be*Cu alloys have been studied with compositions 0.08, 0.41, and 0.78 at.%. Table II presents some of the results of the full calculations for these alloys and where possible compares them

TABLE II. A comparison of observed and calculated dHvA frequencies and cyclotron masses for pure Be and *Be*Cu alloys. The frequencies are given in units of 10^6 G and the masses are relative to a free-electron mass of unity. Each calculation was fitted to the γ_1^1 frequency.

Alloy	Sheet	Branch and field dir. θ	dHvA Frequency Calc	dHvA Frequency Expt	% Diff	Cyclotron mass Calc	Cyclotron mass Expt	Expt/Calc
Pure Be[a]	Cigar	α^1 0°	9.48	9.42 ±0.05	0.6	0.136	0.168 ±0.005	1.24
		α^2 0°	9.75	9.72 ±0.05	0.3	0.142	0.170 ±0.005	1.20
	Coronet	γ_1^1 90°	0.1097	0.110 +0.0006	−0.3	−0.0178	−0.0212 ±0.0006	1.18
		γ_1^2 90°	0.2257	0.226 +0.001	−0.1	−0.0372		
		γ_2^1 90°	0.1270	0.127 ±0.0007	0.0	−0.0207		
		β_1^1 90°	12.41	12.4 ±0.06	0.1	−0.214	−0.260 ±0.009	1.22
		β_2^2 90°	14.86	14.91 ±0.07	−0.3	−0.285	−0.35 ±0.03	1.23
		β_2^2 52°	12.75	12.65 ±0.07	0.8	−0.203	−0.256 ±0.009	1.26
0.08 at.%	Cigar	α^1 0°	9.30	9.25 ±0.05	0.5	0.135	0.179 ±0.009	1.32
		α^2 0°	9.56	9.54 ±0.05	0.2	0.141	0.183 ±0.004	1.30
	Coronet	γ_1^1 90°	0.1284	0.1284 ±0.0009	0.0	−0.0193	−0.0237 ±0.0006	1.23
		γ_1^2 90°	0.265	0.264 ±0.004	−1.5	−0.0402		
		γ_2^1 90°	0.1488	0.150 ±0.002	−0.7	−0.0224		
		β_1^1 90°	12.65	12.60 ±0.06	0.4	−0.214		
		β_2^2 90°	15.20			−0.291		
		β_2^2 53°	12.98	13.01 ±0.07	−0.2	−0.206		
0.41 at.%	Cigar	α^1 0°	8.59			0.131		
		α^2 0°	8.84	8.84 ±0.09	0.0	0.137		
	Coronet	γ_1^1 90°	0.2225	0.222 ±0.002	0.0	−0.0254		
		γ_2^1 90°	0.258	0.257 ±0.002	0.4	−0.0293	−0.036 ±0.002	1.23
		β_1^2 90°	16.59			−0.307		
0.78 at.%	Cigar	α^1 0°	7.95			0.127		
		α^2 0°	8.17			0.132		
	Coronet	γ_1^1 90°	0.3299	0.332[b]		−0.0308		
		γ_2^1 90°	0.3830	0.383 ±0.002	0.0	−0.0359	−0.043 ±0.002	1.20

[a]Data from Ref. 1.

[b]Value based on γ_2^1 assuming secant behavior of the γ branch.

with experimental observations. To give a clearer impression of the changes produced by alloying, we have prepared Table III showing frequency differences, both as observed and as calculated by various methods.

The most striking observation from Table II is that the accuracy with which the alloy frequencies are predicted by the model is as great as for the pure metal. This is rather surprising considering the approximations entailed. Except in following the angular variation of the sensitive neck (γ) frequency branch, the differences always remain less than 1%. A possible explanation of this accuracy may be found by examining Table III. In the next to the last column, we have estimated the shift in frequency simply from the fixed-band terms of Eq. (6), using quantities from pure Be. In calculating ΔE, the Cu atoms are assumed to supply one conduction electron and to produce no change in the calculated $n(E)$. It is now clear that most of the change produced by alloying is due to the electron-concentration effect, so that if the Fermi level can once be well established, a reasonable estimate of the frequencies will be obtained. The other changes in the pseudopotential discussed in Sec. III therefore need to account for only a small fraction of the shift. For this reason, the approximations used are probably adequate. The crucial step is to fix the Fermi level by fitting a known frequency.

Table III shows that, although the fixed-band model is surprisingly good in most cases, the deviations from the observed values become greater as the concentration increases. This is due partly to the sensitivity of the fixed-band model to η. The full calculation, as we have noted, is relatively insensitive to η, which enters only through the lattice spacings. The value of ΔE used in Eq. (6), however, depends directly on η and the results show that if η were slightly lower than the nominal value for the most concentrated alloy and somewhat higher for the others, we could secure better agreement. While the necessary changes would all lie within our uncertainty in the determination of atomic concentration, it is equally probable that other factors, such as screening, might influence the electron concentration. It is interesting to note that Eq. (6) would not be much improved by including higher-order terms in the Taylor expansion. This is because the $(\Delta E)^2$ term itself is significant only for the γ frequencies, and from the form of the energy bands near the coronet necks [linear $E(k)$ curves] we can show that the coefficient of $(\Delta E)^3$ vanishes to the accuracy of our calculation. Similarly, the higher-order strain derivatives are negligible.

The family of γ frequencies arises from a nearly cylindrical portion of the FS as discussed in I. There, significant deviations from cylindrical behavior begin to appear at angles greater than 60° from the cylinder axis. If the FS expands as the electron concentration is reduced, we would expect to find the ratio between the alloy frequency and pure-beryllium frequency to be independent of angle. Such behavior was observed for the alloys studied here although decreasing signal to noise limits the comparison to an angular range of approximately 60° from the cylinder axis. Figure 2 illustrates the constancy of this scaling for the 0.08 at.% alloy where the γ_3^2 frequency is less than 3% above secant dependence at 60° from $\langle 11\bar{2}0\rangle$.

In Fig. 3, we compare the measured α and β families of frequencies from the 0.08 at.% alloy with the frequencies in pure beryllium. In pure Be, the pseudopotential model was successful in following these frequency branches as θ varies out from the symmetry axes. Although the model was not used to compute the angular variation of these branches in the alloys, it is reasonable to assume that it would trace out the experimental curve satisfactorily, since, as we see from Table II, the frequencies in the symmetry directions are accurately obtained.

The model has been used to explore the possibility of magnetic breakdown and its modifications of the observable dHvA frequencies. For ex-

TABLE III. Changes in dHvA frequencies upon alloying. Observed values of $(f_{\text{alloy}} - f_{\text{pure}})$ are compared with values from the full calculation, from the fixed-band term of Eq. (6), and from the complete expression. Units are 10^6 G.

Alloy	Field direction θ and branch	Experiment	Full nonlocal calculation	Fixed-band model	Complete Eq. (6)
0.08%	α^1 0°	−0.17 ±0.08	−0.187	−0.150	−0.156 ±0.002
	α^2 0°	−0.18 ±0.08	−0.185	−0.156	−0.162 ±0.002
	γ_1^1 90°	0.0184±0.0013	0.0187	0.0205	0.0172±0.0008
0.41%	α^2 0°	−0.88 ±0.1	−0.912	−0.789	−0.82 ±0.01
	γ_1^1 90°	0.112 ±0.002	0.112	0.1240	0.106 ±0.004
0.78%	γ_1^1 90°	0.222[a]	0.220	0.2760	0.240 ±0.02

[a]Value based on γ_2^1 assuming secant behavior of the γ branch.

ample, Table II points out that in the 0.41 at.% alloy there was only one frequency present with observable amplitude from the cigar (field along [0001]), whereas the model predicts two which differ still by about 3%. We note further that according to the model, the beat frequency remains essentially constant over the small range of concentrations used, while the cigar cross sections themselves have shrunk by approximately 20%. Thus, it suggests that the α^2 orbit lying out of the symmetry plane persists as the dominant frequency while the α^1 orbit is strongly attenuated by magnetic breakdown. Use of Chambers's formula[6] for the breakdown field H_0 between α^1 and the coronet yields a value of 50 kG for the 0.41 at.% alloy. While this field is not sufficiently low to account for the complete unobservability of the beat frequency under the experimental conditions (the beat pattern at high fields should actually become unobservable at a breakdown field of about 25 kG), the effect is undoubtedly in the right direction. Furthermore, there is sufficient uncertainty in the details of the model, for example, the precision of locating the T_1, T_4 band crossing (I, Table V) to permit a somewhat lower value of H_0.

It is unfortunate that scattering reduces the α oscillations below the noise level in the 0.78 at.% alloy since the model shows the cigar waists to be still present, with an H_0 of 15 kG. Finally, we have computed the variation with Cu concentration of ak,[7] the cigar-coronet separation along ΓK. This is shown in Fig. 4, where the plot is practically linear, and suggests that the two sheets would touch at about 1.2 at.% Cu.

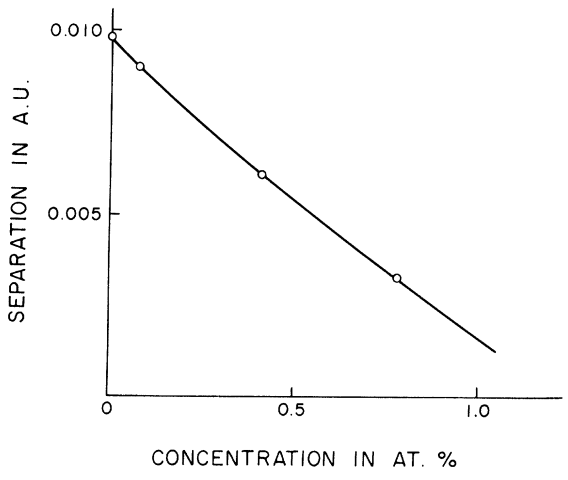

FIG. 4. Variation of the cigar-coronet separation with alloy concentration as measured along ΓK. This is the distance ak illustrated in Fig. 2 of Ref. 1.

Because the model predicts a reduction of the breakdown field with increased copper concentration, we have also used it to investigate several combination orbits which might arise due to magnetic breakdown. The availability of this model is important in estimating the probability of observing such orbits, particularly when symmetry does not require the combination orbit with extremal area to pass through the region of minimum breakdown field. An example of a combination orbit, which by symmetry does pass through such a region, occurs for H in the $\langle 11\bar{2}0\rangle$ plane, enclosing the cigar and the coronet "belly." This should yield a difference frequency of $\beta_2^2 - \alpha_2^1$. Such frequencies are rather unlikely to appear in pure beryllium because of the large breakdown field but might begin to appear in alloys if scattering and a large cyclotron mass do not reduce the amplitude too severely. No such low-frequency oscillations were observed over the field range used in either pure beryllium or in the alloys.

A similar breakdown orbit might occur for H in the $\langle 10\bar{1}0\rangle$ plane, where it would traverse two or three of the coronet bellies and the cigar waist. Calculations indicate that for θ near 40° (a near-optimum location) a broad extremal band of combination orbits occurs with a net area lying close to $2\beta_1^2 - \alpha_1^1$. However, the model also shows that the tunneling point from cigar to coronet lies about 0.04 a.u. out of the ΓKM plane and therefore the breakdown field for this orbit is considerably higher than for the symmetrically disposed orbit discussed above. Again, no dHvA frequencies which might be ascribed to these orbits were seen either in the alloys or the pure metal. A similar combination orbit has been proposed by Alekseevski and Egorov[8] to explain some of their galvanomagnetic data, but it is clear that such an orbit cannot exhibit the sort of angular variation required by their data over the range $20° < \theta < 40°$.

Finally, the very limited amount of data in Table II indicates that mass enhancement in alloys is only slightly, if at all, greater than in pure beryllium. Uncertainties in both experimental and observed masses unfortunately prevent any firm conclusions as to the magnitude of this effect.

V. CONCLUSION

The nonlocal pseudopotential model which was applied so successfully to pure Be has been adapted to provide a description of dilute *Be*Cu alloys. The only unknown parameter of the alloy is the Fermi level which can be obtained by fitting to a known dHvA frequency. When this is done, the model predicts the whole FS as accurately as for the pure metal.

The model has been used to interpret the absence

of one of the α branches from the experimental data. An explanation in terms of magnetic breakdown seems most plausible.

The fixed-band model, which considers only the changes due to electron-concentration effects, indicates that the bulk of the dHvA frequency shift is due to the reduction in the number of conduction electrons. This may explain why the model fits alloys so well, but despite this, the other effects of alloying also appear to be adequately represented in the model: The full calculation shows considerable improvement over the simple fixed-band-model results.

ACKNOWLEDGMENTS

The authors gratefully acknowledge the assistance of Professor J. P. G. Shephard and of Dr. Derek Parsons in the early stages of this work; the helpful suggestions of Professor R. W. Stark, Professor L. M. Falicov, and Professor P. Soven; and the cooperation of Dr. G. London in the preparation of alloy samples and in providing alloy lattice parameters.

*Work supported in part by the Air Force Office of Scientific Research under Grant No. AF AFOSR 536-66 and 69-1637 to Case Western Reserve University, Cleveland, Ohio.

†Present address: Department of Physics, University of Connecticut, Storrs, Conn. 06268.

‡NASA Predoctoral Trainee. Present address: Department of Physics, The Louisiana State University, Baton Rouge, La.

[1]J. H. Tripp, P. M. Everett, W. L. Gordon, and R. W. Stark, Phys. Rev. 180, 669 (1969), to be referred to as I.

[2]P. M. Everett, thesis, Case Western Reserve University, 1968 (unpublished); Cryogenics (to be published).

[3]W. A. Harrison, *Pseudopotentials in the Theory of Metals* (Benjamin, New York, 1966).

[4]O. P. Gupta, Phys. Rev. 174, 668 (1968).

[5]L. Nordheim, Ann. Physik 9, 607 (1931).

[6]R. G. Chambers, Proc. Phys. Soc. (London) 88, 701 (1966).

[7]See Fig. 2 of I for caliper designations.

[8]N. E. Alekseevski and V. S. Egorov, Zh. Eksperim. i Teor. Fiz. 55, 1153 (1968) [Soviet Phys. JETP 28, 601 (1969)].

PHYSICAL REVIEW B VOLUME 2, NUMBER 6 15 SEPTEMBER 1970

Occupied Band Structure of Cu: Soft-X-Ray Spectrum and Comparison with Other Deep-Band-Probe Studies

R. C. Dobbyn, M. L. Williams, J. R. Cuthill, and A. J. McAlister
Institute for Materials Research, National Bureau of Standards, Washington, D. C. 20234

(Received 4 March 1970)

We report a new measurement of the soft-x-ray $M_{2,3}$ emission spectrum of Cu, using improved experimental techniques. Previously unreported fine structure was observed in the spectrum. Although exact correction for satellite and subband overlap and self-absorption effects is not yet possible, careful consideration has been given to them, with the result that the M_3 band profile can be resolved from the accompanying structure in a plausible way. Its features can be taken with reasonable confidence to be characteristic of the true M_3 profile. Comparison is made with the complementary L_3 soft-x-ray profile, with band-theoretical estimates of both experimental x-ray profiles, and with the results of ultraviolet-photoemission, x-ray–photoemission, and ion-neutralization measurements. These comparisons favor a single-particle description of the occupied bands of Cu.

I. INTRODUCTION

Increasingly detailed and realistic calculations of the band structure of the 3*d* metals are becoming available. Notable success has been achieved in predicting the results of experiments which probe electronic structure at the Fermi level. However, such work yields only a limited indication of the validity of single-particle band theory.[1] A full test requires experimental data covering the full range of occupied band structure. To this end, optical, soft-x-ray (SXS), ultraviolet-photoemission (UPS), x-ray–photoemission (XPS), and ion-neutralization (INS) spectroscopies are available. Until recently, only crude agreement has been found among these various experiments, and between such experiments and theory. Many often marked discrepancies have occurred. Even now, it is not completely clear to what extent these arise from purely experimental difficulties on the one hand, or to dif-